Steroidal glycoalkaloids contribute to anthracnose resistance in *Solanum lycopersicum*

Matthew L. Fabian[1], Chong Zhang[1], Jianghao Sun[2], Neil P. Price[3], Pei Chen[3], Christopher R. Clarke[1], Richard W. Jones[1], and John R. Stommel[1]

[1] Genetic Improvement for Fruits and Vegetables Laboratory, Beltsville Agricultural Research Center, U.S. Department of Agriculture-Agricultural Research Service, Beltsville, MD 20705, USA

[2] Methods and Application of Food Composition Laboratory, Beltsville Agricultural Research Center, U.S. Department of Agriculture-Agricultural Research Service, Beltsville, MD 20705, USA

[3] Renewable Product Technology Research, National Center for Agricultural Utilization Research, U.S. Department of Agriculture-Agricultural Research Service, Peoria, IL 61604, USA

author e-mail addresses:

- Matthew L. Fabian: matthew.fabian@usda.gov
- Chong Zhang: woodyzc@gmail.com
- Jianghao Sun: jianghao.sun@usda.gov
- Neil P. Price: neil.price@usda.gov
- Pei Chen: pei.chen@usda.gov
- Christopher R. Clarke: christopher.clarke@usda.gov
- Richard W. Jones: richard.jones@usda.gov
- John R. Stommel: john.stommel@usda.gov

Date of submission:

Word Count: 4,120

Figure count: 5

Supplementary figure count: 7

Supplementary table count: 3

Highlight

This work describes an important role for steroidal glycoalkaloids (SGAs), abundant secondary metabolites in tomato fruit, in defense against anthracnose, a widespread fungal disease that impacts diverse crop species.

Abstract

Anthracnose is a widespread plant disease caused by various species of the fungal pathogen *Colletotrichum*. In solanaceous plants such as tomato (*Solanum lycoperiscum*), *Colletotrichum* infections exhibit a quiescent, asymptomatic state in developing fruit, followed by a transition to necrotrophic infections in ripe fruit. Through analysis of fruit tissue extracts of 95L368, a tomato breeding line that yields fruit with enhanced anthracnose resistance, we identified a role for steroidal glycoalkaloids (SGAs) in anthracnose resistance. The SGA α-tomatine and several of its derivatives accumulated at higher levels, in comparison to fruit of the susceptible tomato cultivar US28, in 95L368 fruit extracts with fungistatic activity against *Colletotrichum*. Correspondingly, ripe and unripe 95L368 fruit displayed enhanced expression of glycoalkaloid metabolic enzyme (GAME) genes, which encode key enzymes in SGA biosynthesis. Metabolomics analysis incorporating recombinant inbred lines (RILs) generated from 95L368 and US28 yielded strong positive correlations between anthracnose resistance and accumulation of α-tomatine and several derivatives. Lastly, transient silencing of expression of the GAME genes *GAME31* and *GAME5* in anthracnose-susceptible tomato fruit yielded enhancements to anthracnose resistance. Together, our data support a role for SGAs in anthracnose defense in tomato, with a distinct SGA metabolomic profile conferring resistance to virulent *Colletotrichum* infections in ripe fruit.

Keywords

anthracnose, Colletotrichum, GAME2, GAME31, GAME4, GAME5, metabolomics, Solanum lycopersicum, steroidal glycoalkaloids, tomato

Abbreviations

GAME:	glycoalkaloid metabolic enzyme
MALDI-TOF:	matrix-assisted laser desorption/ionization time-of-flight
MS:	mass spectrometry
SGA:	steroidal glycoalkalkoid
UHPLC:	ultra-high performance liquid chromatography

Introduction

Anthracnose is a global plant disease caused by *Colletotrichum* spp., hemibiotrophic fungal pathogens with a wide and diverse host range, including a variety of commercially important monocot and dicot crops such as tomato, maize, strawberry, and soybean (Dias et al., 2019; Jacobs et al., 2019; Prochno et al., 2016; Stommel and Haynes, 1998). Plant pathogens in both the field and post-harvest, *Colletotrichum* spp. encompass approximately 190 species in eleven species complexes, exhibiting multiple infection strategies in various types of plant tissue, including foliar, fruit, and root tissue, depending on the pathosystem (Baroncelli et al., 2017; Boufleur et al., 2021; Jayawardena et al., 2016). In solanaceous crops such as pepper and tomato, anthracnose is caused primarily by the species *C. coccodes*, *C. gloeosporioides*, *C. dematium*, and *C. acutatum*, and is characterized by the formation of necrotrophic lesions on fruit (Chapin et al., 2006; Harp et al., 2014; Pardo-De la Hoz et al., 2016). *Colletotrichum*

infections of tomato fruit exhibit a transition from quiescence to virulence during fruit ripening, yielding anthracnose symptoms on ripe fruit. After overwintering in soil, sclerotia form conidia capable of germinating on immature fruit, resulting in an asymptomatic, quiescent state characterized by the formation of appressoria that are restricted to the cuticle. As infected fruit ripens, *Colletotrichum* forms hyphae that penetrate the pericarp, and produces circular depressions that progress into necrotrophic lesions on mature, ripe fruit (Alkan et al., 2015; Peres et al., 2005; Sanogo et al., 2003). In the field, traditional strategies to mitigate anthracnose infection, such as fungicide application, provide incomplete protection, thus the development of genetic tools to improve anthracnose resistance is of particular interest (Byrne et al., 1997; Wyenandt et al., 2009). Anthracnose resistance has been identified in fruits of unadapted tomato germplasm, and attempts to breed this trait into elite materials convey a polygenic, additive mode of inheritance, as well as difficulty in transfer to commercial cultivars with an intensity equal to that observed in the resistant germplasm (Stommel, 2001; Stommel and Haynes, 1998). Therefore, more targeted approaches to develop enhanced anthracnose resistance in commercial cultivars are desirable.

Steroidal glycoalkaloids (SGAs) are secondary metabolites, derived from the mevalonate biosynthetic pathway and characterized by a nitrogenous aglycone backbone and variable glycone sidechains at the C-3 position, that accumulate to high levels in solanaceous plants such as tomato, eggplant, and potato (Cárdenas et al., 2015; You and Kan, 2021; Zhao et al., 2021). Found in various plant tissues, including leaves, fruit, and tubers, some SGAs are generally classified as antinutritional compounds due to the observed toxicity in humans, when ingested at high levels, but SGAs have also been described for their potential health benefits, including anti-inflammatory, anticarcinogenic, and antioxidative properties (Friedman, 2006, 2013; Wang et al., 2018). For example, in vitro and mouse model studies have reported activation of cancer cell apoptosis and reduction of tumor cell growth following treatments of α-tomatine, the most abundant SGA in tomato leaves and green fruit (Chao et al., 2012; Kim et al., 2015). Furthermore, numerous studies have characterized α-tomatine in responses to diverse sources of biotic stress in *Solanaceae* (Hoagland, 2009; Sandrock and VanEtten, 1998). Antifungal activity of α-tomatine was observed in vitro and in tomatoes infected with *Fusarium oxysporum*, a vascular fungal pathogen and the causal agent of fusarium wilt (Ito et al., 2007; Pareja-Jaime et al., 2008), and α-tomatine was shown to restrict in vitro growth of *Phytophthora infestans*, the oomycete pathogen that causes late blight in potato (Dahlin et al., 2017; Sandrock and VanEtten, 1998). Notably, a role for α-tomatine in defense against *Colletotrichum spp.* has been described, with α-tomatine treatment observed to restrict the growth of both *C. coccodes* and *C. acutatum*, and a transgenic tomato line with attenuated levels of α-tomatine displaying enhanced susceptibility to *C. coccodes* (Itkin et al., 2011; Sandrock and VanEtten, 1998). Accordingly, SGAs, including α-tomatine, are of particular interest in the development of genetic tools to imbue enhanced levels of defense against anthracnose and other biotic diseases of tomato.

While α-tomatine accumulates to high levels in immature fruit, levels of α-tomatine and certain derivative SGAs decline together during ripening, ultimately giving way to the derivative esculeosides, end products of the SGA pathway that accumulate tFig. o high levels in ripe fruit. GLYCOALKALOID METABOLIC ENZYME (GAME) genes encode enzymes that catalyze reactions in the SGA pathway (Fig. S1) (Akiyama et al., 2019; Cárdenas et al., 2019; Lee et al., 2019; Nakayasu et al., 2020; Sonawane et al., 2018). The UDP-glycosyltransferase GAME2 catalyzes the synthesis of α-tomatine, as well as the closely related dehydrotomatine, representing a branch point for the synthesis of downstream SGA derivatives (Iijima et al., 2013; Itkin et al., 2013; Kozukue et al., 2004). As tomato fruit ripens, these compounds are converted to derivative SGAs via additional GAME proteins with hydroxylation, acetyltransferase, and glycosylation activities. For example, *GAME31* encodes a 2-oxoglutarate-dependent dioxygenase (2-ODD) that synthesizes hydroxytomatine and hydroxy-dehydrotomatine from α-tomatine and dehydrotomatine, respectively (Nakayasu et al., 2020; Szymański et al., 2020). Additional, as-yet-undiscovered GAME proteins catalyze the acetoxylation of these substrates, respectively forming the derivative acetoxytomatine and acetoxy-dehydrotomatine, and the subsequent hydroxylation reactions that result in the formation of acetoxy-hydroxytomatine and acetoxy-hydroxy-dehydrotomatine, accordingly (Cárdenas et al., 2015; Zhao

et al., 2021). The uridine diphosphate (UDP) glycosyltransferase GAME5 synthesizes the formation of esculeoside A and dehydro-esculeoside A from acetoxy-hydroxytomatine and acetoxy-hydroxy-dehydrotomatine, respectively (Iijima et al., 2009; Nakayasu et al., 2020; Szymański et al., 2020). Although the ripening process in tomato is generally characterized by a decline in α-tomatine levels and coincident accumulation of the end-product esculeosides, comparisons of commercial tomato cultivars, wild tomato accessions, and derivative introgression lines have illustrated a diversity of SGA metabolomic profiles in ripe red fruit, with some lines exhibiting high levels of α-tomatine in both green and red fruit (Dzakovich et al., 2021; Iijima et al., 2013; Szymański et al., 2020; Zhu et al., 2018). While a growing body of evidence supports a role for α-tomatine in pathogen defense, little is known of the contributions of derivative SGAs, therefore germplasm of variant SGA metabolomic profiles can be particularly useful in further research to elucidate the role of SGAs in disease resistance in tomato.

Here our work incorporates an anthracnose-susceptible tomato cultivar (US28) and a small-fruited, commercially unadapated and anthracnose-resistant accession (95L368), as well as a population of twenty-eight selected recombinant inbred lines (RILs), in a study of the relationship between anthracnose defense and the SGA metabolome. Red fruit tissue extracts of the anthracnose-resistant 95L368 exhibited fungistatic activity against *Colletotrichum* and were found to be enriched in certain SGAs. Correspondingly, gene expression analysis conveyed modulated transcription of GAME genes in 95L368 in both green and red fruit. US28, 95L368, and the descendant RILs displayed variable anthracnose resistance, and metabolomics analysis of this population yielded a distribution of SGA profiles in red fruit. Further analysis of the SGA metabolic profiles identified positive correlations between anthracnose resistance and the α-tomatine and dehydrotomatine derivatives hydroxytomatine, acetoxytomatine, and dehydro-acetoxytomatine. Lastly, Virus-Induced Gene Silencing (VIGS) was employed to evaluate the roles of *GAME31* and *GAME5* in anthracnose resistance, wherein silencing of these GAME genes conferred enhanced levels of anthracnose resistance in a susceptible tomato line. Together, these data provide meaningful insights into the contribution of SGAs to anthracnose defense in tomato, highlighting new targets for the development of crop plants with enhanced biotic disease resistance.

Materials and Methods

Plant material and *Colletotrichum* inoculations

The F2 population derived from a cross between the parent lines *Solanum lycopersicum* US28 and 95L368 (formerly denoted 115-4) was generated as described (Stommel, 2001). Twenty-eight recombinant inbred lines (RILs) were selected from a larger RIL population developed via single seed descent from the F2 generation, with each RIL carried to the F6 or F7 generation. Seedlings for US28, 95L368 and the population of 28 RILs were germinated in greenhouse conditions transferred to the field, and arranged into four planting blocks, in Keyport fine loam soil, at USDA-ARS BARC-WEST, Beltsville MD, USA Fruit were harvested at the young, mature green, breaker, and mature red stages, and stored, either whole or diced, at -80 ^{o}C for subsequent experiments. For *Colletotrichum* infection assays, mature red fruit from each line (mean n = 22 fruit per block per line) were harvested and transferred to a greenhouse. *Colletotrichum* isolate C9, previously isolated from tomato in Beltsville and tentatively identified as *C. nigrum*, was maintained and prepared as previously described (Stommel and Haynes, 1998). Suspensions were diluted to a final concentration of 5 x 10^6 spores mL^{-1} for inoculation. Fruit exocarp was wounded via 27-gauge needle, inoculated with a 10 µL droplet of fungal suspension, and incubated in the greenhouse, with lesion diameter (lesion size $\geq$ 1 mm) recorded at 7 dpi, and where noted, converted to “severity” via normalization to the within-block maximum lesion size.

Colletotrichum growth inhibition assays

171 Approximately 300 mg red ripe fruit tissue from 95L368 samples stored at -80 °C was ground with
172 liquid nitrogen in a mortar and pestle, left to thaw, then centrifuged at 13,000 rpm for one minute, after
173 which the supernatant was collected. Supernatant was vortexed and centrifuged with equal parts sterile
174 water and 100% MeOH, and samples of whole supernatant, MeOH fraction, water fraction, and MeOH
175 (control) were spread on V8 agar plates. Spores of *Colletotrichum* C9 were harvested from V8 agar plates
176 and suspended in chilled, sterile water, at a final concentration of 5 x 10^3 µL. Aliquots of 10 µL of fungal
177 suspension were added to the PDA plates and incubated at 25 °C for five days for observation of mycelial
178 growth. For the TLC bioassay, 300 mg samples of lyophilized ripe fruit tissue were homogenized in liquid
179 nitrogen, transferred to 10 mL 100% MeOH, and shaken at 250 rpm for 30 minutes. After centrifugation at
180 5,000 rpm for 15 minutes, 4 mL supernatant was added to 6 mL water, then passed through pre-conditioned
181 (6 mL 100% MeOH followed by 6 mL water) C18 Sep-Pak Cartridges (Waters Corporation, Milford MA,
182 USA) by gravity. After washing with 6 mL 100% MeOH, the samples were eluted with 15 mL 80% MeOH,
183 dried via rotary evaporator, and resuspended in 3 mL 100% MeOH. Aliquots of 10 µL were spotted onto
184 TLC plates and developed at room temperature. After drying the plates in a fume hood for 1 hour, the plates
185 were photographed under UV light, then sprayed with a suspension of *Colletotrichum* C9 (3 x 10^6 spores
186 mL^{-1}) in sterile water and stored in closed petri dishes for 4-5 days before observation of mycelial growth.
187 For the growth inhibition assay incorporating US28, 95L368, and the 4 select RILs, non-treated V8 agar
188 plates were inoculated with *Colletotrichum* as described, and at 7 dpi, 80 µL of MeOH extractions were
189 spotted along the plate perimeters, after which images were generated at 3 and 4 days post-treatment (dpt).
190
191 **SGA Metabolomics**
192
193 For MALDI-TOF MS, fruit tissue methanol extractions separated by C18 chromatography were
194 prepared as previously described. Mass spectra were acquired in positive ion detection mode on a Bruker-
195 Daltonics Microflex spectrometer (Bruker-Daltonics, Billerica MA, USA) For each sample, 2 µL of eluate
196 was mixed with matrix (2,5-dihydrobenzoic acid) in 10 µL acetonitrile and added to 10 µL water, after which
197 0.5 µL spots of the eluate-matrix mix were added to the stainless-steel target surface and crystallized at
198 room temperature. Each sample was measured in triplicate, with 3,000 laser pulses (λ = 337.1 nm) at 200
199 ns each, and with the following voltage settings: ion source 1 19.0 kV; ion source 14.0 kV; lens 9.2 kV; and
200 reflector 20.0 kV. Data was processed via the supplied Bruker Daltonics software, and accurate masses
201 were verified via SIS Exact Mass Calculator (https://www.sisweb.com/referenc/tools/exactmass.htm).
202 For UHPLC-HRMS full scanning, fruit tissue methanol extractions separated by C18
203 chromatography were prepared as previously described. The UHPLC-HRAM MS system consisted of an
204 LTQ Orbitrap XL MS with an Agilent 1290 UHPLC (Agilent Technologies, Santa Clara CA, USA). Separation
205 was conducted on a Hypersil Gold AQ RP-C18 UHPLC column (Thermo Fisher Scientific, Waltham MA,
206 USA) with an UltraShield pre-column filter (Analytical Scientific Instruments, Richmond CA, USA). Gradient
207 elution (Solution A, 0.1% v/v formic acid in water; Solution B, 0.1% formic acid in acetonitrile) was conducted
208 at a flow rate of 0.3 $mL \cdot min^{-1}$. The linear gradient was as follows: increase from 2% to 10% Solution B (v/v)
209 at 10 minutes; increase to 40% Solution B at 25 minutes; increase to 75% Solution B at 30 minutes; increase
210 to 90% Solution B at 50 minutes; and hold at 90% Solution B to 60 minutes. The re-equilibration time for
211 the initial gradient was 5 minutes. Column compartment temperature was set at 50 °C. Data were acquired
212 under positive ionization mode and negative ionization mode with mass range of m/z = 100-2,000 with a
213 resolution of 30,000, separately. The optimized conditions for positive ionization mode were set as follows:
214 sheath gas 80 AU; aux and sweep gas 15 AU; spray voltage 4.5 kV; capillary temperature 325 °C; capillary
215 voltage 40 V; tube lens voltage 150 V; FTMS AGC target 5 x 10^5; FT-MS/MS AGC target 2 x 10^5; isolation
216 width 1.5 atomic mass units (amu); and max ion injection time 200 ms. For negative ionization mode, the
217 parameters were set as follows: spray voltage 4 kV; capillary voltage -50 V; and tube lens voltage -120 V.
218 The most intense ion was selected for the data-dependent scan to observe their MS2 to MS4 product ions,
219 respectively, with a normalization collision energy at 35%.

220 For targeted analysis of SGAs via UHPLC-HRMS, samples of 100 mg lyophilized red fruit tissue
221 were ground in a bead homogenizer with 1/4”-diameter ceramic spheres (MP Biomedicals, LLC, Irvine CA,
222 USA) and vortexed in 5 mL 100% MeOH for 10 seconds. Samples were shaken for 30 minutes at 250 rpm,
223 then centrifuged for 15 minutes at 5,000 rpm, at room temperature. For each sample, approximately 4 mL
224 supernatant was passed through 0.45 µM PTFE syringe filters, then stored at -20 ^{o}C. Injection volumes of
225 1 µL were loaded onto a Q-Exactive mass spectrometer with a Thermo Fisher Vanquish UHPLC system.
226 Separation was conducted on an Agilent Poroshell HPH-C18 column. Gradient elution (Solution A, 0.1%
227 v/v formic acid in water; Solution B, 0.1% v/v formic acid in acetonitrile) was conducted with a flow rate of
228 0.3 mL $\cdot$min^{-1}, a sample compartment temperature of 5 ^{o}C, and a column temperature of 40 ^{o}C. Mass
229 spectra were generated via electrospray ionization with 4 kV spray voltage, an ion transfer tube temperature
230 of 320 ^{o}C, and a scan range of m/z 120-1,800 Da. Ion chromatograms were constructed for the protonated
231 molecular ions of each analyte via high resolution ion extraction with a mass width of 0.01 amu, and the
232 SGA contents (µg g dry weight (DW)$^{-1}$) for all analytes were semi-quantitated as α-tomatine equivalent from
233 an external calibration curve of α-tomatine standard (Sigma-Aldrich, St. Louis MO, USA). For statistical
234 analyses, the SGA content values were $\log_{10}$-transformed via the following formula: $\log_{10}$-SGA = $\log_{10}$ [(x
235 µg gDW^{-1})+1)].
236
237 **Gene expression analysis**
238
239 Fresh-frozen or lyophilized samples of approximately 100 mg fruit tissue were ground in liquid
240 nitrogen in a mortar and pestle, or via bead homogenizer with 1/4”-diameter ceramic spheres (MP
241 Biomedicals, LLC, Irvine CA, USA). RNA was purified via RNEasy Mini Kit (Qiagen, Hilden DE), per
242 manufacturer’s instructions, with elutions in 30 µL RNase-free water. cDNA synthesis was conducted via
243 ProtoScript II First Strand cDNA Synthesis Kit (New England Biolabs, Ipswich MA, USA), using
244 manufacturer’s instructions for reverse transcription of total RNA. RNA masses and purities were analyzed
245 via a DeNovix DS-11 spectrophotometer (DeNovix Inc., Wilmington DE, USA). cDNA samples were diluted
246 100-fold for qRT-PCR. Primers for qRT-PCR were designed from target mRNA sequences, spanning
247 introns where possible, and synthesized by Integrated DNA Technologies, Inc. (Coralville IA, USA); see
248 Table S3 for a list of all primer sequences. Primers for GAME-VIGS qRT-PCR validation were designed to
249 yield amplicons without overlap to the VIGS target amplicons (see below). Primer efficiencies, specificities,
250 and optimal annealing temperatures were analyzed via CFX Maestro Software Version 2.2 (Bio-Rad). qRT-
251 PCR was carried out via an iProof SYBR Green Supermix kit (Bio-Rad Laboratories, Hercules CA, USA)
252 per manufacturer’s instructions. Two technical replicates were included for each sample. For each target
253 relative expression (RE) was calculated via the 2^{-ddCt} method, with the lowest-expression sample
254 designated as the calibrator.
255
256 **Virus-Induced Gene Silencing (VIGS) cloning and GAME-VIGS Agroinfiltration**
257
258 RNA and cDNA were isolated from fresh-frozen 95L368 fruit tissue samples as described above.
259 Primers designed to amplify a 406-bp region of *GAME31* coding sequence (CDS), as well as a 478-bp
260 region of *GAME5* CDS, were synthesized by Integrated DNA Technologies and are listed in Table S3.
261 Amplification of target amplicons with the addition of 5’ XbaI and 3’ BamHI restriction enzyme digestion
262 sites was carried out on a Bio-Rad T100 thermocycler (Bio-Rad Laboratories, Hercules CA, USA) via Bio-
263 Rad iProof High Fidelity DNA Polymerase using manufacturer’s instructions. Amplicons were separated via
264 gel electrophoresis on a Bio-Rad PowerPac Basic system, analyzed via an Azure c150 Gel Imaging System
265 (Azure Biosystems, Inc., Dublin CA, USA), and purified via Zymoclean Gel DNA Recovery kit (Zymo
266 Research, Irvine CA, USA) using manufacturer’s instructions. The bipartite VIGS system consisted of the
267 vectors pYL192 (TRV1) and pYL156 (TRV2). Double digestion of pYL156 and target amplicons was
268 conducted via Thermo Fisher FastDigest BamHI and XbaI using manufacturer’s instructions. Ligations

269 utilized New England Biolabs T4 ligase and were conducted at 16 °C overnight, followed by enzyme
270 deactivation at 65 °C for 10 minutes. Aliquots of 2 µL of each reaction were added to 50 µL high efficiency
271 New England Biolabs 5-alpha Competent *E. coli*, placed on ice for 30 minutes, incubated in a 42 °C water
272 bath for 40 seconds, then returned to ice for 2 minutes. After recovery in 1 mL LB for 1 hour, cells were
273 washed in 100 µL LB, plated on LB agar supplemented with 50 µg/mL kanamycin, and incubated at 38 °C
274 overnight. Positive clones were identified via PCR as previously described, using MangoMix Taq DNA
275 polymerase (Meridian Bioscience Inc., Cincinnati OH, USA) and manufacturer's instructions.
276 Putatively recombinant plasmid was isolated from overnight cultures using the Zymo Research
277 ZymoPURE Plasmid Miniprep Kit, per manufacturer's instructions. Positive recombinant vector was verified
278 via Sanger sequencing incorporating the NOS-R primer (Table S3) and performed by Psomagen (Rockville
279 MD, USA). Aliquots of 1 µL of TRV1 and recombinant TRV2 were electroporated into 50 µL tubes of
280 *Agrobacterium tumifasciens* strain GV3101 cells (Intact Genomics, St. Louis MO, USA) using a Bio-Rad
281 Gene Pulser II and Pulse Controller electroporation system set to 2.2 kV. Transformants were grown on LB
282 plates supplemented with 50 µg mL^{-1} kanamycin and 25 µg mL^{-1} spectinomycin and verified via PCR; see
283 Table S3 for primers. For agroinfiltration, 5 mL overnight cultures in LB supplemented with 50 µg mL^{-1}
284 kanamycin were transferred to 20 mL cultures and shaken at 225 rpm for 3 hours or until an approximate
285 OD_{600} of 1.0 was reached, then pelleted and resuspended in 20 mL infiltration medium (200 µL 1M $MgCl_2$
286 + 200 µL 1M MES pH 5.6 + 20 µl 200 mM acetosyringone + 19.58 mL sterile water). After gentle shaking
287 for 3 hours, 1:3 TRV1:TRV2 mixed suspensions were prepared. Micro Tom tomato plants grown in
288 greenhouse conditions and presenting immature green fruit were agroinoculated via the Agrodrench
289 method, in which 5 mL of 1:3 TRV1:TRV2 suspensions were aliquoted to root crowns (Ryu et al., 2004). At
290 22 dpi, this process was repeated for a second dose of GAME-VIGS Agrodrench. At 41 days following the
291 initial dose, mature red tomatoes were harvested for *Colletotrichum* C9 inoculation and lesion size
292 measurement as previously described.
293
294 **Data analysis and software**
295
296 Statistical significance was determined via one-way Student's T-test or ANOVA with post-hoc
297 Tukey testing, as noted, using Microsoft Excel or R Studio version 2021.09.0 with R version 4.1.1, with the
298 "multcompView" package, as appropriate. Bar plots were generated in R with the "ggpubr" package.
299 Correlograms were generated, including determination of Pearson correlation coefficients, in R via the
300 "ggally" package. Scatterplots were generated in R via the "ggplot2" package. Heatmaps were generated
301 in R via the "pheatmap" package. Plasmid maps were generated in Geneious Prime version 2022.0.1.
302
303 **Results**
304
305 **Tissue extracts of an anthracnose-resistant, wild tomato accession convey fungicidal activity**
306 **against *Colletotrichum***
307
308 To evaluate the respective levels of anthracnose resistance in US28 and 95L368, ripe fruit were
309 harvested, inoculated with *Colletotrichum*, and scored for lesion diameter at 9 dpi (Fig. S2a). We observed
310 characteristic anthracnose lesions in US28 fruit, however 95L368 fruit were minimally symptomatic and in
311 total, displayed a 33-fold decrease in lesion size when compared to US28 (Fig. 1a-b). We sought to
312 determine whether the enhanced anthracnose resistance exhibited by ripe 95L368 fruit was the result of
313 antifungal, biochemical activity in fruit tissue. Utilizing whole supernatant, water-extracted, and methanol-
314 extracted fruit tissue samples supplemented onto PDA plates, we observed a restriction of mycelial growth
315 on plates supplemented with whole supernatant or methanol-extracted fraction, indicative of fungistatic
316 activity of polar compounds that accumulate in 95L368 fruit (Fig. 1c). To further validate these findings,
317 methanol extractions of US28 and 95L368 ripe fruit were separated via TLC, after which a suspension of

318 *Colletotrichum* C9 (3 x 10^6 spores mL^{-1}) was sprayed onto the TLC plate. At 3-4 dpi, a zone of inhibition
319 around the polar phase of 95L368 fruit tissue extract was observed (Fig. S2b). Together, these findings
320 suggested that one or more polar compounds that accumulate in 95L368 red fruit possess fungistatic
321 activity against *Colletotrichum*, thereby contributing to anthracnose resistance.
322
323 **Ripe fruit tissue of the anthracnose-resistant accession 95L368 is enriched in the production of α-**
324 **tomatine and several α-tomatine derivatives**
325
326 To identify compounds that contribute to enhanced anthracnose resistance in 95L368, we
327 conducted a pilot study of phase-separated polar extracts of ripe US28 and 95L368 red fruit tissue. Tissue
328 extracts were separated via TLC as described, and the regions of the TLC plate corresponding to the zone
329 of inhibition of *Colletotrichum* growth (Fig. S2b) were analyzed via HPLC-MS. In a comparison of the total
330 ion chromatograms (TICs) generated for 95L368 and US28 samples we identified elution of several
331 steroidal glycoalkaloids (SGAs) in the retention time range of 20-25 minutes (Fig. 2a; Fig. S3). Additionally,
332 TICs of US28 red fruit displayed a peak at 19.9 minutes that was identified as esculeoside A (*m*/*z* =
333 1,270.61). Notably, this peak was absent in TICs of 95L368, which instead displayed strong peaks at 23.1
334 and 22.7 minutes, indicative of an enrichment of α-tomatine (*m*/*z* = 1,034.55) and the derivative
335 hydroxytomatine (*m*/*z* = 1,092.56), respectively.
336 We next sought to evaluate the distribution of several key SGAs in green, breaker (intermediate
337 ripening), and ripe red fruit. Methanol extractions of tissue samples from US28 and 95L368 fruit were
338 analyzed via matrix-assisted desorption/ionization time-of-flight (MALDI-TOF) mass spectrometry. In the
339 resulting spectrogram for US28, we observed signals (*m*/*z* ≈ 1,034 and 1,056), indicative of an accumulation
340 of α-tomatine ($C_{50}H_{83}NO_{21}$) and its sodium adduct ion in both green and breaker fruit (Fig. 2b). As expected,
341 these α-tomatine signals were also detected in breaker fruit, but not in red ripe fruit, while both breaker and
342 red fruit yielded signals (m/z ≈ 1,270 and 1,292) corresponding to the major and sodium adduct ions of
343 esculeoside A, consistent with the working model for SGA biochemistry in ripening tomato fruit.
344 Interestingly, an unidentified compound yielded suspected major (m/z ≈ 1,213) and sodium adduct (m/z ≈
345 1,236) ions, perhaps indicative of deacetoxylated esculeoside A or dehydroxylated esculeoside B
346 ($C_{56}H_{92}NO_{27}$; MW = 1,211.32), in both breaker and red fruit samples from US28. Analysis of the spectra for
347 green and breaker fruit tissue of 95L368 identified an accumulation of α-tomatine, however, in contrast to
348 US28, α-tomatine was also detected in ripe fruit tissue (Fig. 2c). Additionally, esculeosides were not
349 observed in the spectra for breaker and red fruit samples of 95L368; instead, these samples yielded strong
350 signals (m/z ≈ 1,093 and 1,115) identified as the major and sodium adduct ions for acetoxytomatine, the
351 most proximal derivative of α-tomatine in the SGA metabolic pathway.
352
353 **GAME genes are variably expressed in anthracnose-susceptible and -resistant cultivars**
354
355 Because we observed that fruit of the anthracnose-resistant 95L 368 accumulated α-tomatine and
356 hydroxytomatine in both green and red fruit, whereas these compounds decline in ripe fruit of anthracnose-
357 sensitive US28, giving way to the derivative esculeosides, we surveyed the expression of GAME genes,
358 which encode enzymes in the SGA biosynthetic pathway, in both green and red fruit of US28 and 95L368.
359 Overall expression of *GAME4* and *GAME2* declined in the transition from green to red fruit, and in a
360 comparison to US28 green fruit, we observed 95L368 green fruit to exhibit 37.4- and 17.7-fold higher
361 expression of *GAME4* and *GAME2,* respectively (Fig. 2d). Interestingly, red 95L368 fruit were characterized
362 by 2.7-fold higher expression of *GAME31*, as well as a 4.6-fold depletion of *GAME5* transcripts, when
363 compared to red US28 fruit. This expression profile of GAME genes in anthracnose-resistant 95L368
364 supports our observation of enhanced accumulation of α-tomatine and acetoxytomatine in both green and
365 red fruit, as well as the depletion of esculeosides in red ripe fruit.
366

367 **SGA metabolic profiles correlate with anthracnose resistance in RILs developed from a cross**
368 **between US28 and 95L368**
369
370 Previous work in our laboratory utilized a tomato population developed from crosses between US28
371 and multiple different anthracnose-resistant breeding lines, including 95L368, to characterize the heritability
372 of anthracnose resistance (Stommel, 2001; Stommel and Haynes, 1998). Because anthracnose resistance
373 was determined to be a polygenic trait, we evaluated a population of twenty-eight recombinant inbred lines
374 (RILs), developed from a cross between US28 and 95L368, that exhibit variety in anthracnose susceptibility.
375 This population, as well as the parent lines US28 and 95L368, were surveyed for *Colletotrichum* resistance,
376 yielding a distribution of mean lesion diameters ranging from 0.39 to 11.33 mm (Fig. 3; Table S1). Next, we
377 profiled the SGA metabolomes of this population. Methanol extractions separated and analyzed via
378 UHPLC-HRMS yielded mean total SGA levels between 137.21 and 58,929.66 µg g dry weight^{-1}, with peaks
379 corresponding to α-tomatine, as well as peaks putatively identified as five SGA derivatives of α-tomatine:
380 multiple isomers of hydroxytomatine (*m*/*z* = 1,050.55); acetoxytomatine (*m*/*z* = 1,092.56); acetoxy-
381 dehydrotomatine (*m*/*z* = 1,090.54); esculeoside A (*m*/*z* = 1,270.61); and esculeoside B (*m*/*z* = 1,228.60)
382 (Table S2; Fig. S4). To evaluate the potential contributions of individual SGAs to anthracnose resistance,
383 we performed correlation analyses on anthracnose susceptibility and SGA levels. Due to variance in overall
384 anthracnose disease severity across planting blocks (Fig. S2; Table S1), lesion diameter values in each
385 planting block were transformed to "severity" values by normalizing to the maximum lesion size in that block.
386 Pearson correlation coefficients for severity and the $\log_{10}$-transformed SGA measurements conveyed
387 negative correlations ($-0.5 \leq R^2 \leq -0.68$) between disease severity and the SGAs α-tomatine,
388 hydroxytomatine, acetoxytomatine, and dehydro-acetoxytomatine, with hydroxytomatine levels yielding the
389 strongest correlation ($R^2 = -0.68$) (Fig. 4a-b; Fig. S5). Among the SGAs measured, hydroxytomatine,
390 acetoxytomatine, and dehydro-acetoxytomatine exhibited strong positive correlations ($0.73 \leq R^2 \leq 0.97$)
391 with each other, as did esculeoside A and esculeoside B ($R^2 = 0.69$).
392 To survey the distribution of anthracnose disease severity and accumulation of the individual SGAs
393 at the level of individual RILs and parent lines, we generated a heat map with RILs ordered by increasing
394 anthracnose severity. Interestingly, the six most anthracnose-resistant RILs (99L 444, 99L 391, 99L 1-14,
395 99L 394, 99L 334, and 99L 313) exhibited a pattern of relative enrichment in hydroxytomatine,
396 acetoxytomatine, and dehydro-acetoxytomatine. Conversely, nine most anthracnose-susceptible RILs (99L
397 375, 99L 437, 99L 453, 99L 424, 99L 314, 99L 395, 99L 418, 99L 473, and 99L 1-28) were relatively
398 depleted of these analytes and possessed relatively higher levels of the esculeosides (Fig. 4c). Of the SGAs
399 most positively correlated with anthracnose resistance, only hydroxytomatine has been characterized for
400 synthesis by a corresponding GAME gene (*GAME31*). To investigate whether modulated expression of
401 GAME genes is associated with enrichment or depletion of SGAs in RILs, we selected two highly
402 anthracnose-resistant (99L444 and 99L391) and -susceptible (99L453 and 99L375) RILs for GAME gene
403 expression analysis and observed variable enrichment of *GAME2* and *GAME31* transcripts in the selected
404 anthracnose-resistant RILs (Fig. S6a). Additionally, methanol extractions of US28, 95L368, and the four
405 selected RILs were tested in a plate growth inhibition assay using *Colletotrichum* strain C9, wherein
406 methanol extractions from 95L368 and the two anthracnose-resistant RILs displayed inhibitive activity,
407 restricting mycelial growth at the perimeter of the plate, in contrast to the extractions from anthracnose-
408 susceptible lines, which displayed no effect (Fig. S6b).
409
410 **Targeted silencing of *GAME31* or *GAME5* confers enhanced anthracnose defense**
411
412 Following our observations that tomato fruit with enhanced anthracnose resistance are enriched in
413 α-tomatine, hydroxytomatine, acetoxytomatine, and dehydro-acetoxytomatine, we theorized that targeted
414 gene silencing of select GAME genes would improve resistance to *Colletotrichum* in fruit of susceptible wild
415 type tomato. To that end, we employed a bipartite Virus-Induced Gene Silencing (VIGS) system.

416 Hypothesizing that silencing of *GAME31* would attenuate conversion of α-tomatine to hydroxytomatine,
417 thereby increasing α-tomatine levels, and that silencing of *GAME5* would reduce conversion of SGAs to the
418 esculeosides, we cloned a 406-bp region of *GAME31* coding sequence (CDS) and a 478-bp region of
419 *GAME5* CDS into the pYL156 TRV2 plasmid (Fig. S7). The resulting TRV1-TRV2 vector systems, in
420 addition to a TRV1-TRV2 empty vector system, were introduced to Micro Tom plants with developing fruit
421 via the Agrodrench method (Ryu et al., 2004). Ripe fruit were harvested for *Colletotrichum* infection, and at
422 7 dpi, we observed 4.3-fold and 3.4-fold reductions in mean lesion diameter in *GAME31*-VIGS and *GAME5*-
423 VIGS transformant fruit, respectively, accompanied by 3.6-fold and 2.4-fold reductions in target gene
424 expression (Figure 5).
425
426 **Discussion**
427
428 Anthracnose, caused by the hemibiotrophic fungal pathogen *Colletotrichum spp*., affects a wide
429 array of crop plants in the field and post-harvest, negatively impacting yield and threatening food security
430 in many growing regions across the globe. To date, there have been limited studies providing insights into
431 mechanisms of anthracnose resistance. Here, our work incorporating an anthracnose-resistant tomato
432 breeding line, as well as a population of 28 RILs derived from a cross between anthracnose-resistant and
433 -susceptible parentage, identifies a role for the secondary metabolites known as steroidal glycoalkaloids
434 (SGAs) in anthracnose defense in tomato. Our data illustrates a fungistatic activity against *Colletotrichum*
435 in red ripe fruit tissue extracts of the anthracnose-resistant breeding line 95L368, and through comparative
436 biochemical analysis of 95L368 and the anthracnose-susceptible cultivar US28, an enrichment in ripe
437 95L368 fruit of the SGAs α-tomatine and acetoxytomatine accompanying an absence of the end-product
438 esculeosides. Incorporating the population of RILs in a broader analysis of anthracnose resistance and
439 SGA metabolomic profiles, we identified positive correlations between anthracnose resistance and the α-
440 tomatine derivatives hydroxytomatine and acetoxytomatine, as well as dehydro-acetoxytomatine, a
441 dehydrotomatine derivative, respectively. Enhanced expression of GAME genes, which encode enzymes
442 in SGA biosynthesis, was observed in 95L368 and select anthracnose-resistant RILs, and targeted
443 silencing of *GAME31* and *GAME5* conferred enhanced anthracnose resistance in fruit of susceptible wild
444 type plants. Together, our findings introduce a role for several SGAs, previously shown to accumulate under
445 developmental control during the ripening process in tomato, in defense against anthracnose. Our data
446 further suggest that the transition of SGA profiles underpins the transition of *Colletotrichum* infections from
447 a quiescent state to necrotrophy during tomato fruit ripening.
448 Across our population of anthracnose-resistant and -susceptible parent and RIL lines we observed
449 a distribution of SGA accumulation (Fig. 4; Fig. S5; Table S2), as well as modulation of GAME gene
450 expression, namely enhanced expression of *GAME4*, *GAME2*, and *GAME31*, coincident with enhanced
451 anthracnose resistance (Fig. 3; Fig. S6). Additionally, targeted silencing of *GAME31* and *GAME5* conferred
452 enhanced levels of anthracnose resistance in wild type fruit (Fig. 5; Fig. S7). In tomato fruit, the transition
453 of *Colletotrichum* infections from a quiescent state to necrotrophy coincides with ripening, and our data
454 suggest that favorable variations in GAME gene expression elicit SGA metabolic profiles that enhance
455 anthracnose defense. The nature of the underlying regulation of GAME gene expression remains to be
456 elucidated. However, the ripening process in tomato fruit is characterized by a variety of changes within the
457 host tissue, such as the activation of production and signaling of the phytohormones abscisic acid, ethylene,
458 and jasmonic acid, and accordingly, phytohormones have been characterized for roles in the regulation of
459 SGA biosynthesis in tomato (Alkan et al., 2015; Cárdenas et al., 2015; Pesaresi et al., 2014; Quinet et al.,
460 2019). Research incorporating tomato mutant lines with constitutive production of jasmonic acid, as well as
461 exogenous treatment with methyl jasmonate (MeJA), have yielded enhanced levels of α-tomatine and
462 expression of GAME genes in root and leaf tissue; conversely, leaf tissue from mutant lines with attenuated
463 jasmonic acid production displayed lower levels of α-tomatine and several derivatives, as well as impaired
464 defense against the fungal pathogen *Fusarium oxysporum* (Montero-Vargas et al., 2018; Thagun et al.,

2016). Transcription factors known as jasmonate-responsive transcription factors of the ETHYLENE RESPONSE FACTOR (ERF) family (JREs) interact with JRE-binding elements in gene promoters and have been investigated for their role in the regulation of GAME gene expression. *GAME9*, also known as JRE4, is jasmonic acid-induced and expressed at high levels in various plant tissues, and interacts with the JRE-binding element in the 5' flanking regions of *GAME4* (Thagun et al., 2016; Yu et al., 2020). *JRE4* has also been shown to positively regulate the expression of multiple different GAME genes, and transgenic suppression of *JRE4* in tomato fruit conferred reductions in α-tomatine content in green fruit (Nakayasu et al., 2018; Thagun et al., 2016). Modulation of GAME gene expression, which impacts SGA production and anthracnose defense, may result from variable levels of jasmonic acid signaling and JRE transcription factor activity at key GAME genes. Therefore, to better understand the genetic mechanisms underlying anthracnose defense, future work should seek to assess endogenous jasmonic acid levels, jasmonic acid signaling activity, and GAME gene promoter identity and activity in anthracnose-resistant and -susceptible lines.

Multiple activities explaining the fungistatic activity of SGAs against pathogens have been proposed. Fungistatic activity of tomatidine against the human fungal pathogen *Candida albicans* was shown to occur through the ergosterol pathway, supporting a role for SGAs in membrane disruption of fungal pathogens (Dorsaz et al., 2017). *C. albicans* treated with tomatidine exhibited dose-dependent reductions of ergosterol, as well as inhibition of the sterol methyltransferase Erg6, and mutations in Erg6 were identified from a forward genetics approach utilizing tomatidine-resistant strains. Multiple studies have demonstrated the efficacy of α-tomatine in membrane disruption using liposomes, with reports of specificity of α-tomatine towards 3β-hydroxyl sterols such as ergosterol which, in free form, are present in lower amounts in tomato (Roddick and Drysdale, 1984; Steel and Drysdale, 1988; You and Kan, 2021). Alternatively, the induction of cell death in *Fusarium oxysporum* by α-tomatine was shown to occur via the generation of intracellular reactive oxygen species (ROS), likely through modulation of tyrosine kinase, G protein, and ATP synthase activities (Ito et al., 2007). The tetraose moiety of α-tomatine is important to its biological activity: Tomatinases, produced by various tomato pathogens, are capable of hydrolyzing one or more carbohydrate residues from this moiety, rendering α-tomatine less toxic and thereby contributing to virulence (Ökmen et al., 2013; Pareja-Jaime et al., 2008; Sandrock and VanEtten, 1998). Targeted manipulation of the SGA metabolic pathway and its metabolites may afford opportunities for durable host resistance against pathogen detoxification mechanisms.

We employed VIGS to silence expression of *GAME31* and *GAME5*, respectively targeted to reduce the conversion of α-tomatine to hydroxytomatine and the production of the esculeosides, with both strategies conferring enhanced anthracnose resistance (Fig. 5; Fig. S7). Our results demonstrated fungistatic activities of red tomato fruit tissue extracts possessing high levels of α-tomatine and the derivatives hydroxytomatine, acetoxytomatine, and dehydro-acetoxytomatine, and positive correlations between the accumulation of these compounds and anthracnose resistance in red fruit (Fig. 1-2; Fig. S2-S4; Fig. 4; Table S2). One or more of these derivatives may possess antifungal activity similar to that of α-tomatine, however, no studies have individually examined these α-tomatine derivatives for their antifungal activities. Therefore, future studies might seek to isolate these compounds for structural evaluation of their fungistatic activities against *Colletotrichum* and other fungal pathogens of tomato and other crop species. Furthermore, the targeted manipulation of GAME gene expression presented here can be expanded to develop tomato breeding lines with stable enhancement or suppression of GAME gene expression, with the purpose of generating high levels of SGAs conferring enhanced resistance to *Colletotrichum* and other tomato pathogens. Together, our data demonstrates a role for SGAs, including α-tomatine and certain of its derivatives, as well as GAME genes including *GAME31* and *GAME5*, in anthracnose defense in tomato fruit, findings that can be utilized to further optimize management of tomato pathogens that impact yield.

Supplementary Data

514 Fig. S1. Simplified schematic of the steroidal glycoalkaloid (SGA) metabolic pathway
515 during tomato fruit ripening.
516 Fig. S2. *Colleotrichum* resistance in the tomato accession 95L 368.
517 Fig. S3. 95L 368 accumulates enhanced levels of SGAs.
518 Fig. S4. Representative extracted ion chromatograms (EICs) for detected SGAs.
519 Fig. S5. Mean detected SGAs vs. mean anthracnose disease severity.
520 Fig. S6. Anthracnose-resistant and –susceptible RILs exhibit variable GAME gene
521 expression and *Colletotrichum* growth inhibition.
522 Fig. S7. Transient silencing of *GAME* genes via VIGS.
523 Table S1. Anthracnose resistance distribution among parent lines and RILs.
524 Table S2. SGA measurements (ug gDW^{-1}) among parent lines and RILs.
525 Table S3. PCR primers utilized in this study.
526
527 **Acknowledgements**
528
529 This research was supported by the U.S. Department of Agriculture, Agricultural Research Service.
530 Mention of trade names or commercial products in this publication is solely for the purpose of providing
531 specific information and does not imply recommendation or endorsement by the U.S. Department of
532 Agriculture. USDA is an equal opportunity provider and employer.
533
534 **Author Contributions**
535
536 Fabian, M.L. and Zhang, C. contributed equally to this study.

Literature Cited

Akiyama, R., Lee, H.J., Nakayasu, M., Osakabe, K., Osakabe, Y., Umemoto, N., Saito, K., Muranaka, T., Sugimoto, Y., and Mizutani, M. (2019). Characterization of steroid 5α-reductase involved in α-tomatine biosynthesis in tomatoes. Plant Biotechnol. *36*, 253–263. https://doi.org/10.5511/plantbiotechnology.19.1030a.

Alkan, N., Friedlander, G., Ment, D., Prusky, D., and Fluhr, R. (2015). Simultaneous transcriptome analysis of Colletotrichum gloeosporioides and tomato fruit pathosystem reveals novel fungal pathogenicity and fruit defense strategies. New Phytol. *205*, 801–815. .

Baroncelli, R., Talhinhas, P., Pensec, F., Sukno, S.A., Le Floch, G., and Thon, M.R. (2017). The Colletotrichum acutatum Species Complex as a Model System to Study Evolution and Host Specialization in Plant Pathogens. Front. Microbiol. *8*, 2001. https://doi.org/10.3389/fmicb.2017.02001.

Boufleur, T.R., Ciampi-Guillardi, M., Tikami, Í., Rogério, F., Thon, M.R., Sukno, S.A., Massola Júnior, N.S., and Baroncelli, R. (2021). Soybean anthracnose caused by Colletotrichum species: Current status and future prospects. Mol. Plant Pathol. *22*, 393–409. https://doi.org/10.1111/mpp.13036.

Byrne, J.M., Hausbeck, M.K., and Latin, R.X. (1997). Efficacy and Economics of Management Strategies to Control Anthracnose Fruit Rot in Processing Tomatoes in the Midwest. Plant Dis. *81*, 1167–1172. https://doi.org/10.1094/PDIS.1997.81.10.1167.

Cárdenas, P.D., Sonawane, P.D., Heinig, U., Bocobza, S.E., Burdman, S., and Aharoni, A. (2015). The bitter side of the nightshades: Genomics drives discovery in Solanaceae steroidal alkaloid metabolism. Phytochemistry *113*, 24–32. https://doi.org/10.1016/j.phytochem.2014.12.010.

Cárdenas, P.D., Sonawane, P.D., Heinig, U., Jozwiak, A., Panda, S., Abebie, B., Kazachkova, Y., Pliner, M., Unger, T., Wolf, D., et al. (2019). Pathways to defense metabolites and evading fruit bitterness in genus Solanum evolved through 2-oxoglutarate-dependent dioxygenases. Nat. Commun. *10*, 5169. https://doi.org/10.1038/s41467-019-13211-4.

Chao, M.-W., Chen, C.-H., Chang, Y.-L., Teng, C.-M., and Pan, S.-L. (2012). α-Tomatine-Mediated Anti-Cancer Activity In Vitro and In Vivo through Cell Cycle- and Caspase-Independent Pathways. PLoS ONE *7*, e44093. https://doi.org/10.1371/journal.pone.0044093.

Chapin, L.J.G., Wang, Y., Lutton, E., and Gardener, B.B.M. (2006). Distribution and Fungicide Sensitivity of Fungal Pathogens Causing Anthracnose-like Lesions on Tomatoes Grown in Ohio. Plant Dis. *90*, 397–403. https://doi.org/10.1094/PD-90-0397.

Dahlin, P., Müller, M.C., Ekengren, S., McKee, L.S., and Bulone, V. (2017). The Impact of Steroidal Glycoalkaloids on the Physiology of Phytophthora infestans, the Causative Agent of Potato Late Blight. Mol. Plant-Microbe Interactions® *30*, 531–542. https://doi.org/10.1094/MPMI-09-16-0186-R.

Dias, M.D., Dias-Neto, J.J., Santos, M.D.M., Formento, A.N., Bizerra, L.V.A.S., Fonseca, M.E.N., Boiteux, L.S., and Café-Filho, A.C. (2019). Current Status of Soybean Anthracnose Associated with Colletotrichum truncatum in Brazil and Argentina. Plants *8*, 459. https://doi.org/10.3390/plants8110459.

Dorsaz, S., Snäkä, T., Favre-Godal, Q., Maudens, P., Boulens, N., Furrer, P., Ebrahimi, S.N., Hamburger, M., Allémann, E., Gindro, K., et al. (2017). Identification and Mode of Action of a Plant Natural Product Targeting Human Fungal Pathogens. Antimicrob. Agents Chemother. *61*, e00829-17. https://doi.org/10.1128/AAC.00829-17.

Dzakovich, M.P., Francis, D.M., and Cooperstone, J.L. (2021). Biosynthesis of Steroidal Alkaloids Are Coordinately Regulated and Differ Among Tomatoes in the Red-Fruited Clade. BioRxiv 2021.01.06.425594. https://doi.org/10.1101/2021.01.06.425594.

Friedman, M. (2006). Potato Glycoalkaloids and Metabolites: Roles in the Plant and in the Diet. J. Agric. Food Chem. *54*, 8655–8681. https://doi.org/10.1021/jf061471t.

Friedman, M. (2013). Anticarcinogenic, cardioprotective, and other health benefits of tomato compounds lycopene, α-tomatine, and tomatidine in pure form and in fresh and processed tomatoes. J. Agric. Food Chem. *61*, 9534–9550. https://doi.org/10.1021/jf402654e.

Harp, T., Kuhn, P., Roberts, P.D., and Pernezny, K.L. (2014). Management and cross-infectivity potential of Colletotrichum acutatum causing anthracnose on bell pepper in Florida. Phytoparasitica *42*, 31–39. https://doi.org/10.1007/s12600-013-0334-9.

Hoagland, R. (2009). Toxicity of tomatine and tomatidine on weeds, crops and phytopathogenetic fungi. Allelopathy J. *00*, 425–436. .

Iijima, Y., Fujiwara, Y., Tokita, T., Ikeda, T., Nohara, T., Aoki, K., and Shibata, D. (2009). Involvement of Ethylene in the Accumulation of Esculeoside A during Fruit Ripening of Tomato (Solanum lycopersicum). J. Agric. Food Chem. *57*, 3247–3252. https://doi.org/10.1021/jf8037902.

Iijima, Y., Watanabe, B., Sasaki, R., Takenaka, M., Ono, H., Sakurai, N., Umemoto, N., Suzuki, H., Shibata, D., and Aoki, K. (2013). Steroidal glycoalkaloid profiling and structures of glycoalkaloids in wild tomato fruit. Phytochemistry *95*, 145–157. https://doi.org/10.1016/j.phytochem.2013.07.016.

Itkin, M., Rogachev, I., Alkan, N., Rosenberg, T., Malitsky, S., Masini, L., Meir, S., Iijima, Y., Aoki, K., de Vos, R., et al. (2011). GLYCOALKALOID METABOLISM1 Is Required for Steroidal Alkaloid Glycosylation and Prevention of Phytotoxicity in Tomato[W]. Plant Cell *23*, 4507–4525. https://doi.org/10.1105/tpc.111.088732.

Itkin, M., Heinig, U., Tzfadia, O., Bhide, A.J., Shinde, B., Cardenas, P.D., Bocobza, S.E., Unger, T., Malitsky, S., Finkers, R., et al. (2013). Biosynthesis of Antinutritional Alkaloids in Solanaceous Crops Is Mediated by Clustered Genes. Science *341*, 175–179. https://doi.org/10.1126/science.1240230.

Ito, S., Ihara, T., Tamura, H., Tanaka, S., Ikeda, T., Kajihara, H., Dissanayake, C., Abdel-Motaal, F.F., and El-Sayed, M.A. (2007). α-Tomatine, the major saponin in tomato, induces programmed cell death mediated by reactive oxygen species in the fungal pathogen Fusarium oxysporum. FEBS Lett. *581*, 3217–3222. https://doi.org/10.1016/j.febslet.2007.06.010.

Jacobs, R.L., Adhikari, T.B., Pattison, J., Yencho, G.C., Fernandez, G.E., and Louws, F.J. (2019). Inheritance of Resistance to Colletotrichum gloeosporioides and C. acutatum in Strawberry. Phytopathology® *109*, 428–435. https://doi.org/10.1094/PHYTO-08-18-0283-R.

Jayawardena, R., Hyde, K., Damm, U., Cai, L., Liu, M., Li, X.H., Zhang, W., Zhao, W., and Yan, J. (2016). Notes on currently accepted species of Colletotrichum. *7*, 1192–1260. https://doi.org/10.5943/mycosphere/si/2c/9.

Kim, S.P., Nam, S.H., and Friedman, M. (2015). The Tomato Glycoalkaloid α-Tomatine Induces Caspase-Independent Cell Death in Mouse Colon Cancer CT-26 Cells and Transplanted Tumors in Mice. J. Agric. Food Chem. *63*, 1142–1150. https://doi.org/10.1021/jf5040288.

Kozukue, N., Han, J.-S., Lee, K.-R., and Friedman, M. (2004). Dehydrotomatine and α-Tomatine Content in Tomato Fruits and Vegetative Plant Tissues. J. Agric. Food Chem. *52*, 2079–2083. https://doi.org/10.1021/jf0306845.

Lee, H.J., Nakayasu, M., Akiyama, R., Kobayashi, M., Miyachi, H., Sugimoto, Y., Umemoto, N., Saito, K., Muranaka, T., and Mizutani, M. (2019). Identification of a 3β-Hydroxysteroid Dehydrogenase/ 3-Ketosteroid Reductase Involved in α-Tomatine Biosynthesis in Tomato. Plant Cell Physiol. *60*, 1304–1315. https://doi.org/10.1093/pcp/pcz049.

Montero-Vargas, J.M., Casarrubias-Castillo, K., Martínez-Gallardo, N., Ordaz-Ortiz, J.J., Délano-Frier, J.P., and Winkler, R. (2018). Modulation of steroidal glycoalkaloid biosynthesis in tomato (Solanum lycopersicum) by jasmonic acid. Plant Sci. *277*, 155–165. https://doi.org/10.1016/j.plantsci.2018.08.020.

Nakayasu, M., Shioya, N., Shikata, M., Thagun, C., Abdelkareem, A., Okabe, Y., Ariizumi, T., Arimura, G., Mizutani, M., Ezura, H., et al. (2018). JRE4 is a master transcriptional regulator of defense-related steroidal glycoalkaloids in tomato. Plant J. *94*, 975–990. https://doi.org/10.1111/tpj.13911.

Nakayasu, M., Akiyama, R., Kobayashi, M., Lee, H.J., Kawasaki, T., Watanabe, B., Urakawa, S., Kato, J., Sugimoto, Y., Iijima, Y., et al. (2020). Identification of α-Tomatine 23-Hydroxylase Involved in the Detoxification of a Bitter Glycoalkaloid. Plant Cell Physiol. *61*, 21–28. https://doi.org/10.1093/pcp/pcz224.

Ökmen, B., Etalo, D.W., Joosten, M.H.A.J., Bouwmeester, H.J., de Vos, R.C.H., Collemare, J., and de Wit, P.J.G.M. (2013). Detoxification of α-tomatine by Cladosporium fulvum is required for full virulence on tomato. New Phytol. *198*, 1203–1214. https://doi.org/10.1111/nph.12208.

Pardo-De la Hoz, C.J., Calderón, C., Rincón, A.M., Cárdenas, M., Danies, G., López-Kleine, L., Restrepo, S., and Jiménez, P. (2016). Species from the Colletotrichum acutatum, Colletotrichum boninense and Colletotrichum gloeosporioides species complexes associated with tree tomato and mango crops in Colombia. Plant Pathol. *65*, 227–237. https://doi.org/10.1111/ppa.12410.

Pareja-Jaime, Y., Roncero, M.I.G., and Ruiz-Roldán, M.C. (2008). Tomatinase from Fusarium oxysporum f. sp. lycopersici Is Required for Full Virulence on Tomato Plants. Mol. Plant-Microbe Interactions® *21*, 728–736. https://doi.org/10.1094/MPMI-21-6-0728.

Peres, N.A., Timmer, L.W., Adaskaveg, J.E., and Correll, J.C. (2005). Lifestyles of Colletotrichum acutatum. Plant Dis. *89*, 784–796. https://doi.org/10.1094/PD-89-0784.

Pesaresi, P., Mizzotti, C., Colombo, M., and Masiero, S. (2014). Genetic regulation and structural changes during tomato fruit development and ripening. Front. Plant Sci. *5*. .

Prochno, H.C., Coelho, C. de J., Romanek, C., Silva, D.F.G., Tasior, D., Oliveira, E.A.T., Gardingo, J.R., and Matiello, R.R. (2016). Genetic resistance of maize inbred lines to anthracnose leaf blight. Crop Breed. Appl. Biotechnol. *16*, 55–61. https://doi.org/10.1590/1984-70332016v16n1a9.

Quinet, M., Angosto, T., Yuste-Lisbona, F.J., Blanchard-Gros, R., Bigot, S., Martinez, J.-P., and Lutts, S. (2019). Tomato Fruit Development and Metabolism. Front. Plant Sci. *10*. .

Roddick, J.G., and Drysdale, R.B. (1984). Destabilization of liposome membranes by the steroidal glycoalkaloid α-tomatine. Phytochemistry *23*, 543–547. https://doi.org/10.1016/S0031-9422(00)80377-5.

Ryu, C.-M., Anand, A., Kang, L., and Mysore, K.S. (2004). Agrodrench: a novel and effective agroinoculation method for virus-induced gene silencing in roots and diverse Solanaceous species. Plant J. *40*, 322–331. https://doi.org/10.1111/j.1365-313X.2004.02211.x.

Sandrock, R.W., and VanEtten, H.D. (1998). Fungal Sensitivity to and Enzymatic Degradation of the Phytoanticipin α-Tomatine. Phytopathology® *88*, 137–143. https://doi.org/10.1094/PHYTO.1998.88.2.137.

Sanogo, S., Stevenson, R.E., and Pennypacker, S.P. (2003). Appressorium Formation and Tomato Fruit Infection by Colletotrichum coccodes. Plant Dis. *87*, 336–340. https://doi.org/10.1094/PDIS.2003.87.4.336.

Sonawane, P.D., Heinig, U., Panda, S., Gilboa, N.S., Yona, M., Kumar, S.P., Alkan, N., Unger, T., Bocobza, S., Pliner, M., et al. (2018). Short-chain dehydrogenase/reductase governs steroidal specialized metabolites structural diversity and toxicity in the genus Solanum. Proc. Natl. Acad. Sci. *115*, E5419–E5428. https://doi.org/10.1073/pnas.1804835115.

Steel, C.C., and Drysdale, R.B. (1988). Electrolyte leakage from plant and fungal tissues and disruption of liposome membranes by α-tomatine. Phytochemistry *27*, 1025–1030. https://doi.org/10.1016/0031-9422(88)80266-8.

Stommel, J.R. (2001). Selection Influences Heritability Estimates and Variance Components for Anthracnose Resistance in Populations Derived from an Intraspecific Cross of Tomato. J. Am. Soc. Hortic. Sci. *126*, 468–473. https://doi.org/10.21273/JASHS.126.4.468.

Stommel, J.R., and Haynes, K.G. (1998). Inheritance of Resistance to Anthracnose Caused by Colletotrichum coccodes in Tomato. J. Am. Soc. Hortic. Sci. *123*, 832–836. https://doi.org/10.21273/JASHS.123.5.832.

Szymański, J., Bocobza, S., Panda, S., Sonawane, P., Cárdenas, P.D., Lashbrooke, J., Kamble, A., Shahaf, N., Meir, S., Bovy, A., et al. (2020). Analysis of wild tomato introgression lines elucidates the genetic basis of transcriptome and metabolome variation underlying fruit traits and pathogen response. Nat. Genet. *52*, 1111–1121. https://doi.org/10.1038/s41588-020-0690-6.

Thagun, C., Imanishi, S., Kudo, T., Nakabayashi, R., Ohyama, K., Mori, T., Kawamoto, K., Nakamura, Y., Katayama, M., Nonaka, S., et al. (2016). Jasmonate-Responsive ERF Transcription Factors Regulate Steroidal Glycoalkaloid Biosynthesis in Tomato. Plant Cell Physiol. *57*, 961–975. https://doi.org/10.1093/pcp/pcw067.

Wang, C., Meng, L., Gao, Y., Grierson, D., and Fu, D. (2018). Manipulation of Light Signal Transduction Factors as a Means of Modifying Steroidal Glycoalkaloids Accumulation in Tomato Leaves. Front. Plant Sci. *9*. .

Wyenandt, C.A., Rhodes, L.H., Bennett, M.A., and Riedel, R.M. (2009). Control of Fruit Rots of Processing Tomato Using Cover Crop Mulch and Tom-Cast. HortTechnology *19*, 511–517. https://doi.org/10.21273/HORTSCI.19.3.511.

You, Y., and Kan, J.A.L. van (2021). Bitter and sweet make tomato hard to (b)eat. New Phytol. *230*, 90–100. https://doi.org/10.1111/nph.17104.

Yu, G., Li, C., Zhang, L., Zhu, G., Munir, S., Shi, C., Zhang, H., Ai, G., Gao, S., Zhang, Y., et al. (2020). An allelic variant of GAME9 determines its binding capacity with the GAME17 promoter in the regulation of steroidal glycoalkaloid biosynthesis in tomato. J. Exp. Bot. *71*, 2527–2536. https://doi.org/10.1093/jxb/eraa014.

Zhao, D.-K., Zhao, Y., Chen, S.-Y., and Kennelly, E.J. (2021). Solanum steroidal glycoalkaloids: structural diversity, biological activities, and biosynthesis. Nat. Prod. Rep. https://doi.org/10.1039/D1NP00001B.

Zhu, G., Wang, S., Huang, Z., Zhang, S., Liao, Q., Zhang, C., Lin, T., Qin, M., Peng, M., Yang, C., et al. (2018). Rewiring of the Fruit Metabolome in Tomato Breeding. Cell *172*, 249-261.e12. https://doi.org/10.1016/j.cell.2017.12.019.

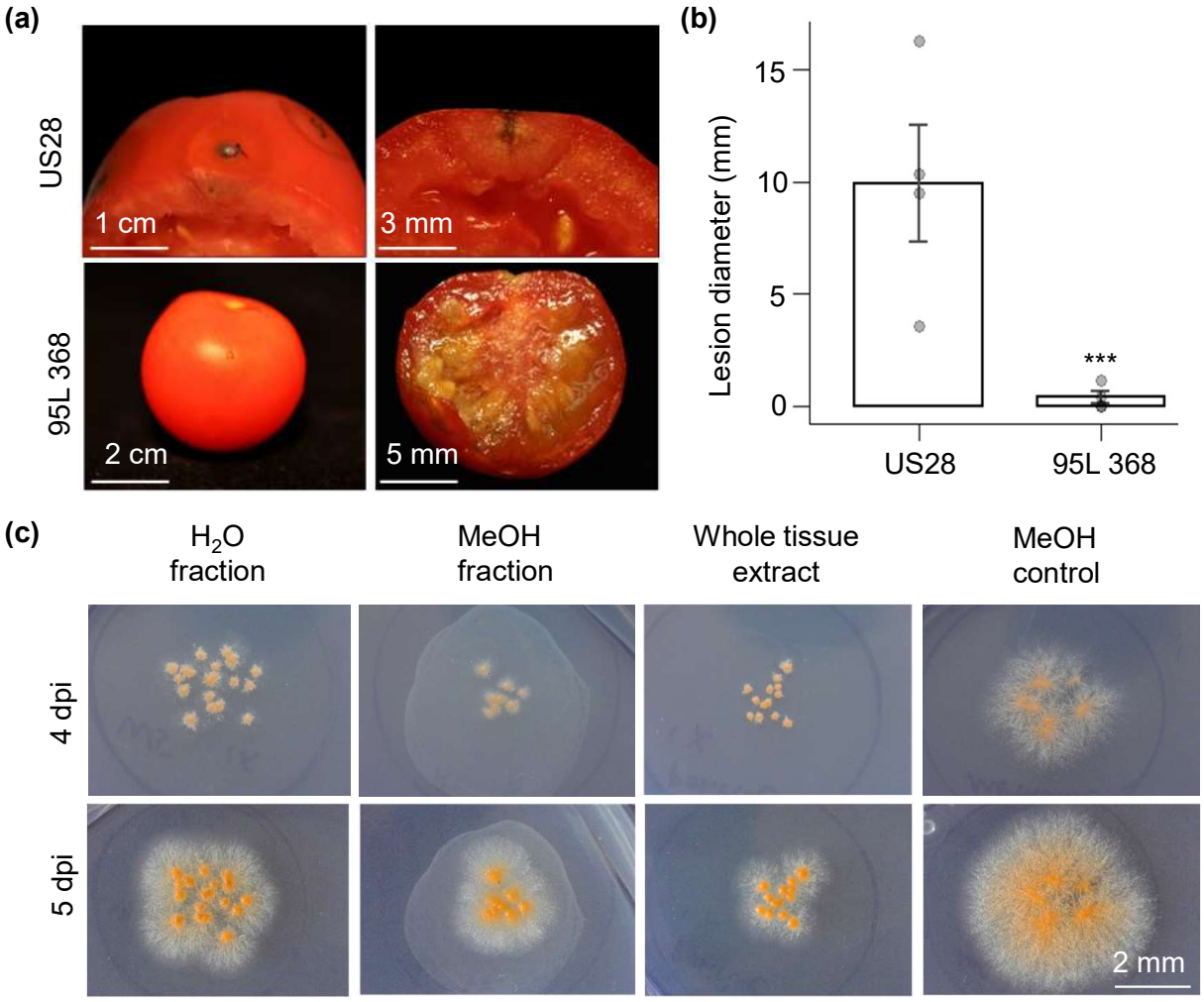

Figure 1. Fruit tissue extracts from an anthracnose-resistant tomato accession exhibit fungistatic activity against *Colleotrichum*. (a) Representative images (9 dpi) of anthracnose-susceptible (US28, top) and resistant (95L 368, bottom) tomato fruit following inoculation with *Colletotrichum*. (b) Lesion diameter following *Colletotrichum* infection. Ripe fruit were harvested and inoculated with *Colletotrichum,* with lesion size measured at 9 dpi. Data points represent average lesion size from each of 4 planting blocks per line, with error bars representing SEM. Asterisks represent statistical significance (one-way Student's T-test). (c) *Colletotrichum* growth inhibition plate assay. H_2O- or MeOH-fractionated and whole extracts from 95L 368 fruit tissue were spotted on PDA plates before inoculation with *Colletotrichum*.

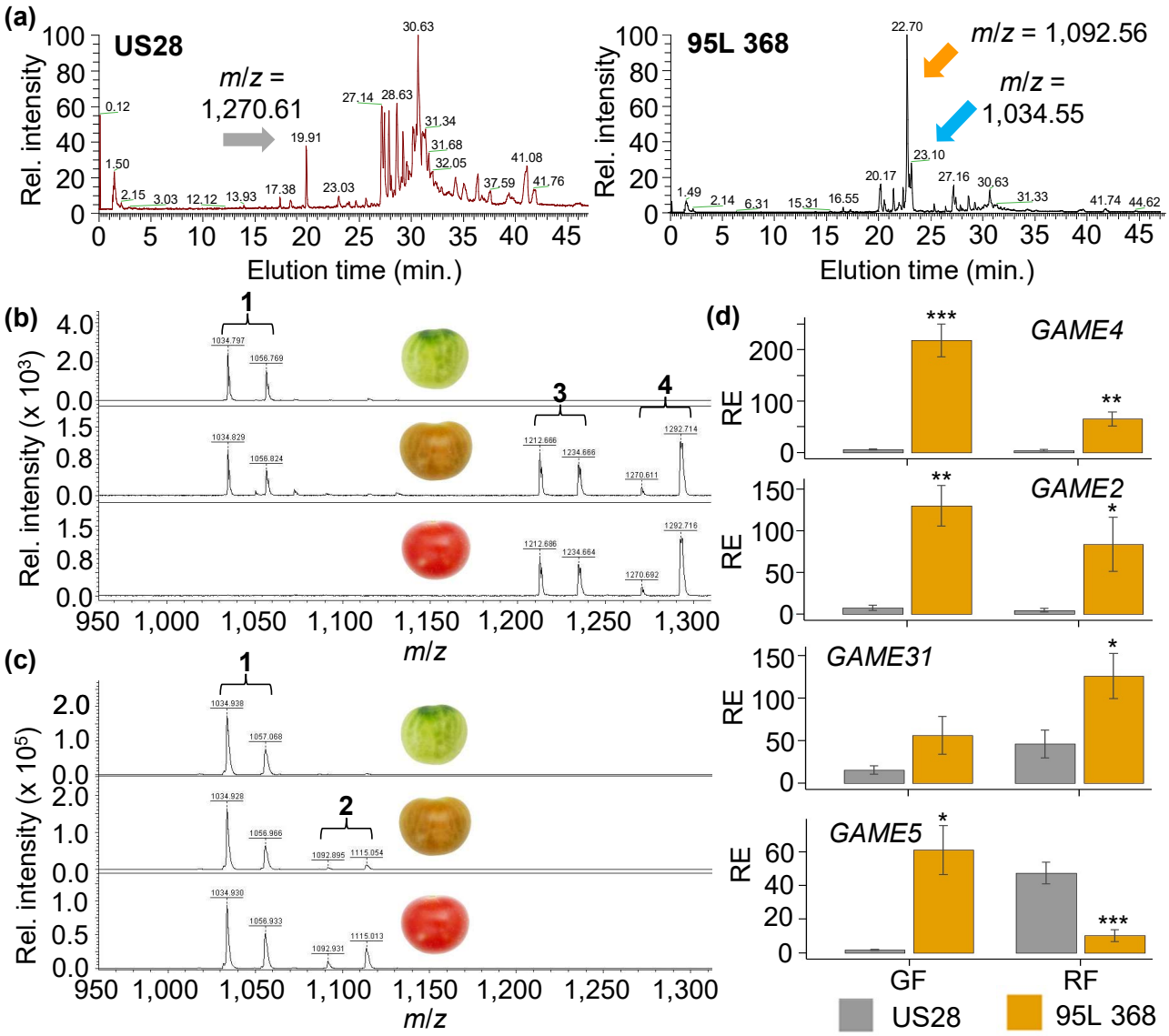

Figure 2. SGA metabolic and *GAME* transcript profiles in green and ripe red fruit of anthracnose-susceptible and –resistant tomato cultivars. (a) Representative TICs from electrospray negative ionization HPLC-MS of ripe red fruit tissue samples of US28 (left) and 95L 368 (right). Arrows indicate peaks corresponding to esculeoside A (grey), α-tomatine (orange), and hydroxytomatine (blue). (b) and (c) Representative chromatograms from MALDI-TOF MS analysis of US28 (b) and 95L 368 (c) fruit tissue by ripening stage. From top to bottom: green fruit, breaker fruit, and red fruit. From left to right: (1) α–tomatine; (2) acetoxytomatine; (3) unknown compound; and (4) esculeoside A. (d) Expression analysis of GAME gene expression in US28 and 95L368 in green (GF, left) and red (RF, right) fruit. qRT-PCR was conducted with 2 technical replicates of 3 biological replicates per sample, in 3 experiments. RE indicates relative expression, asterisks indicate statistical significance (1-way Student's T-test), and error bars represent SEM.

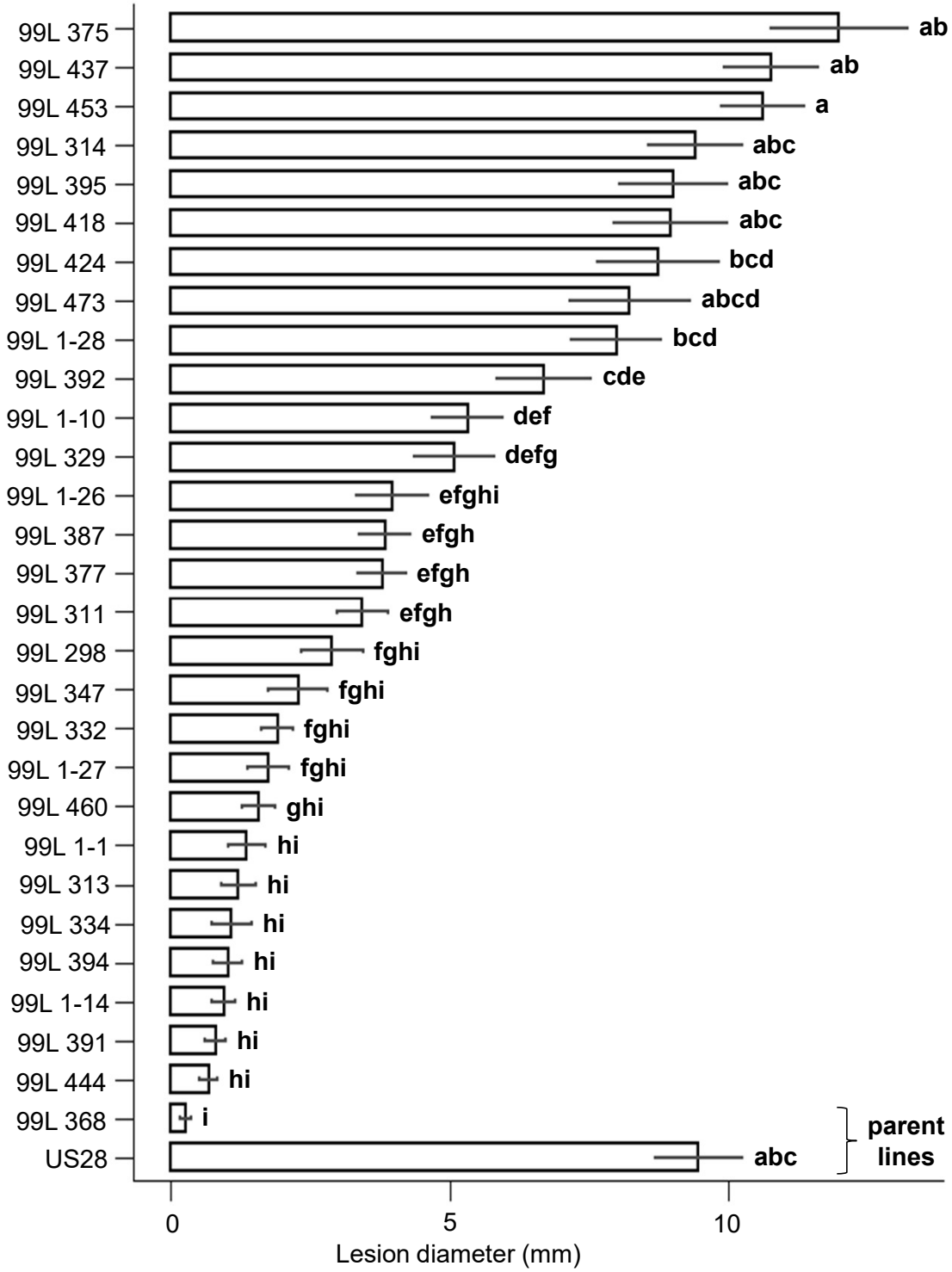

Figure 3. Anthracnose resistance distribution among parent lines and RILs. Ripe red fruit were harvested and inoculated with *Colletotrichum* and incubated in greenhouse conditions, with lesion diameter measured at 9 dpi. Data points represent mean lesion size from each of 4 planting blocks per line, with error bars representing SEM. Statistical significance was determined via ANOVA with post-hoc Tukey testing.

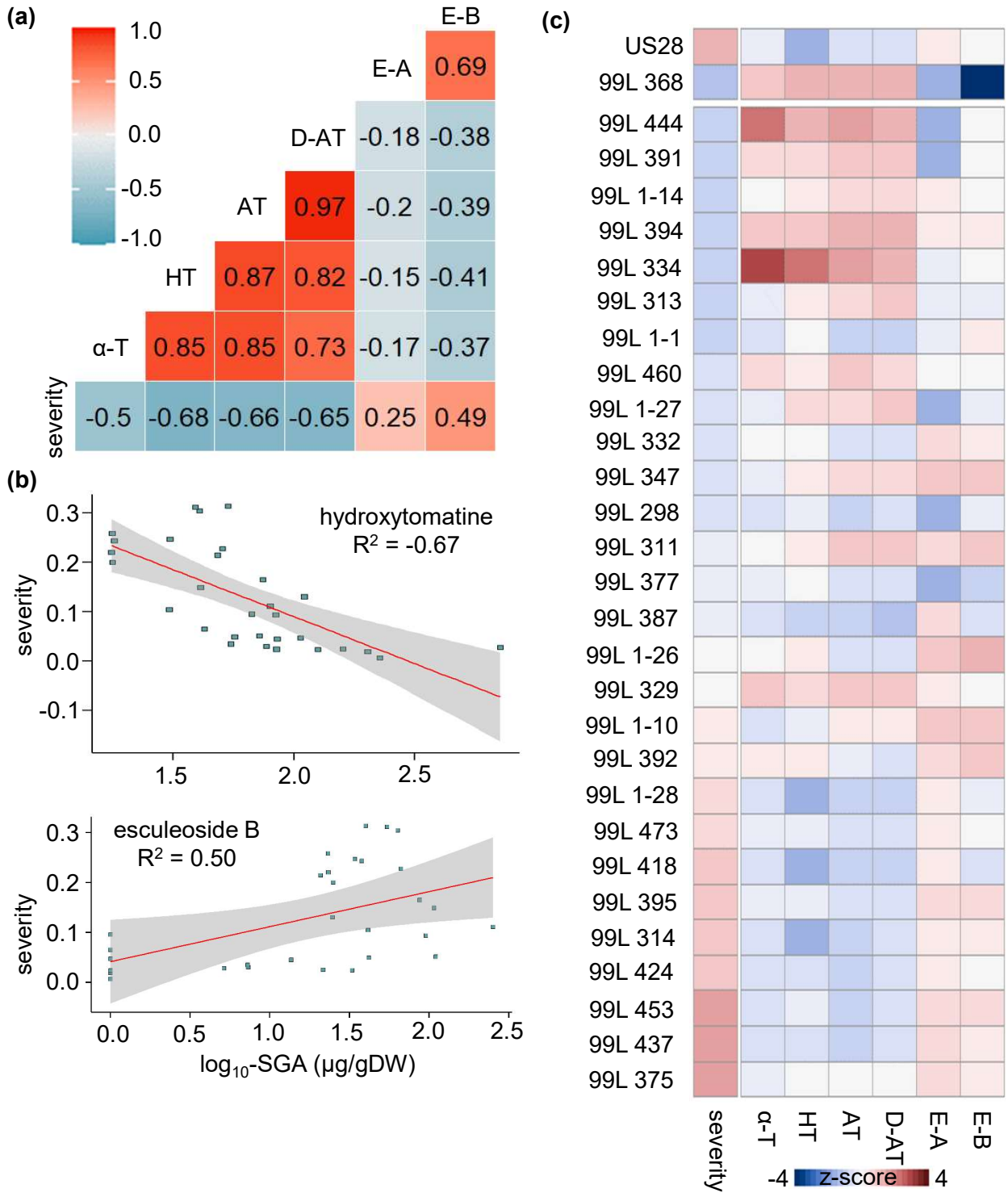

Figure 4. SGAs variably correlate to anthracnose resistance in the parent lines and RIL population. (a) Pearson correlogram of total anthracnose disease severity and SGA levels. (b) Scatterplot of anthracnose severity vs. hydroxytomatine (upper) and esculeoside A (lower) levels with general linear model (GLM) trendline and 95% C.I. Each point corresponds to an individual parent line or RIL. (c) Heat map of z-score-transformed anthracnose severity and SGA levels by parent line and RILs. SGA levels for (a) - (c) are $\log_{10}$-transformed. α–T, α -tomatine. HT, hydroxytomatine. AT, acetoxytomatine. D-AT, dehydro-acetoxytomatine. E-A, esculeoside A. E-B, esculeoside B.

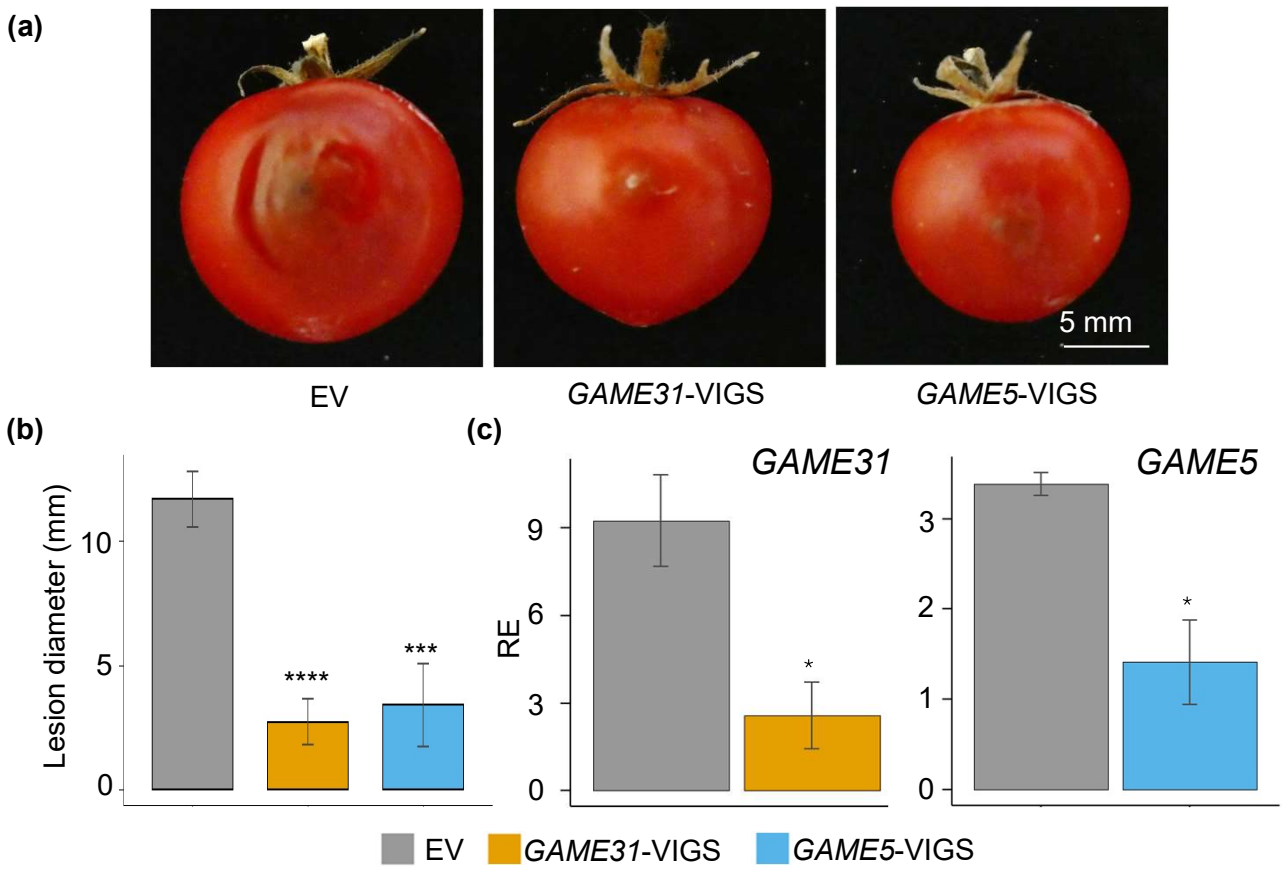

Figure 5. Transient, targeted silencing of *GAME31* and *GAME5* confer enhanced anthracnose resistance in wild type fruit. Bipartite VIGS vectors targeting silencing of *GAME31* or *GAME5* were introduced to Micro Tom plants (n = 2 per treatment) presenting immature green fruit via the Agrodrench method, and mature red fruit were harvested for *Colletotrichum* infection and gene expression via qRT-PCR. (a) Representative images of infected fruit. (b) Lesion diameter of infected fruit ($n \geq 9$). (c) Expression of *GAME31* (left) and *GAME5* (right). Samples from infected fruit were collected at 7 dpi and processed for RNA extraction. For each target, qRT-PCR was conducted with 2 technical replicates of 3 biological replicates per treatment. EV, empty vector control. RE indicates relative expression, asterisks indicate statistical significance (* $p < 0.05$, *** $p < 0.001$, **** $p < 0.0001$, 1-way Student's t-test) and error bars indicate SEM.